

Optical and Electrochemical Properties of PB-ZnO and PB-ZnO/MWCNT Nanocomposite Films Deposited by Chemical Bath

Fatma Özütok^{1,*} and Emin Yakar²

¹Physics Department, Çanakkale Onsekiz Mart University, 17020, Çanakkale, Turkey

²Materials Science and Engineering, Çanakkale Onsekiz Mart University, 17020, Çanakkale, Turkey

Received: September 22, 2017, Accepted: January 06, 2018, Available online: May 07, 2018

Abstract: The first aim of this study was to investigate the ZnO modification effect on the prussian blue (PB) films. A second aim of the study was to determine the decoration effect of multi walled carbon nanotube (MWCNT) on the PB-ZnO nanocomposite films which could be deposited by chemical bath. The electrochemical behaviour of PB films was systematically studied using ZnO- or ZnO/MWCNT modification. Additionally, detailed optical properties of nanocomposite films were determined by UV-VIS, FTIR and Raman spectroscopy. Optical transparency was severely decreased by ZnO modification onto PB film but the decoration of MWCNTs did not change the optical transparency of film compared to PB film. PB, ZnO and MWCNT presence in the nanocomposite films were proven by FTIR spectrum. Stretching vibration peak of C≡N shifted to short-wavelength for PB-ZnO nanocomposite films and same peak disappeared with MWCNT coating due to the structural distortion. ZnO modification and MWCNT coating affected the electrochemical properties due to the different factors such as OH group effect in film growth process, Zn²⁺ substitution with Fe²⁺ site and interaction between ferricyanide ions and oxygen.

Keywords: Prussian blue films, ZnO structure, multi-walled carbon nanotubes, optical properties, electrochemical properties, chemical bath deposition

1. INTRODUCTION

Nowadays, electrochromic (EC) devices are so attractive with and can be used for very different industrial applications such as automotive smart window[1], electrochromic display technology[2] and building isolation [3]. EC devices generally occurs consist of two sided electrolyte/EC material/ transparent conductor/substrate sandwiched structure. The most altering and important part of inorganic EC devices is transparent and conducting electrochromic film e.g. WO₃, NiO, TiO₂ and prussian blue etc. Among them prussian blue (PB) [Fe^{III}₄[Fe^I(CN)₆]₃ · nH₂O (n= 14–16)] as a multi-EC film which has Faradaic four redox states and excellent properties such as uniform coloring and bleaching, high optical contrast and reversible of electrochemical cycles. On the other hand, PB has rapid reaction process and un-controlled reaction kinetics between ferric (Fe³⁺) and ferricyanide (Fe(CN)₆)⁴⁻ ions are uncontrolled therefore its capability of PB film decreases

to use it as anand PB-based EC device performance still need further improve.

In order to improve to efficiency as an EC film of PB for EC film applications, mixing is so preferred with the proper materials that have been high specific surface area and porous surfaces is preferred. PB mixing films that contain metal oxide structures (Fe₂O₃, TiO₂, SnO₂ etc.) has been extensively studied [4-5]. Among them ZnO is ideal candidate with tuning and beneficial properties such as large band gap energy (3.37 eV), high transparency in Uv-Vis region (T%>75) and good catalysis performance for photochemical reactions. However, ZnO nanocrystals are grown in alkaline solution whereas PB nanocrystals are grown in acidic medium and hence material quality of PB-ZnO nanocomposite might be decreased. To overcome this problem, additional materials such as graphene, single walled carbon nanotube and multi walled carbon nanotube can be used to stabilize the chemical reactions and to ease reversible electron transfer. C-based materials and, multi walled carbon nanotubes (MWCNTs) greatly en-

*To whom correspondence should be addressed: Email: fatmaozutok@comu.edu.tr
Phone: +90 286 2180018/1942

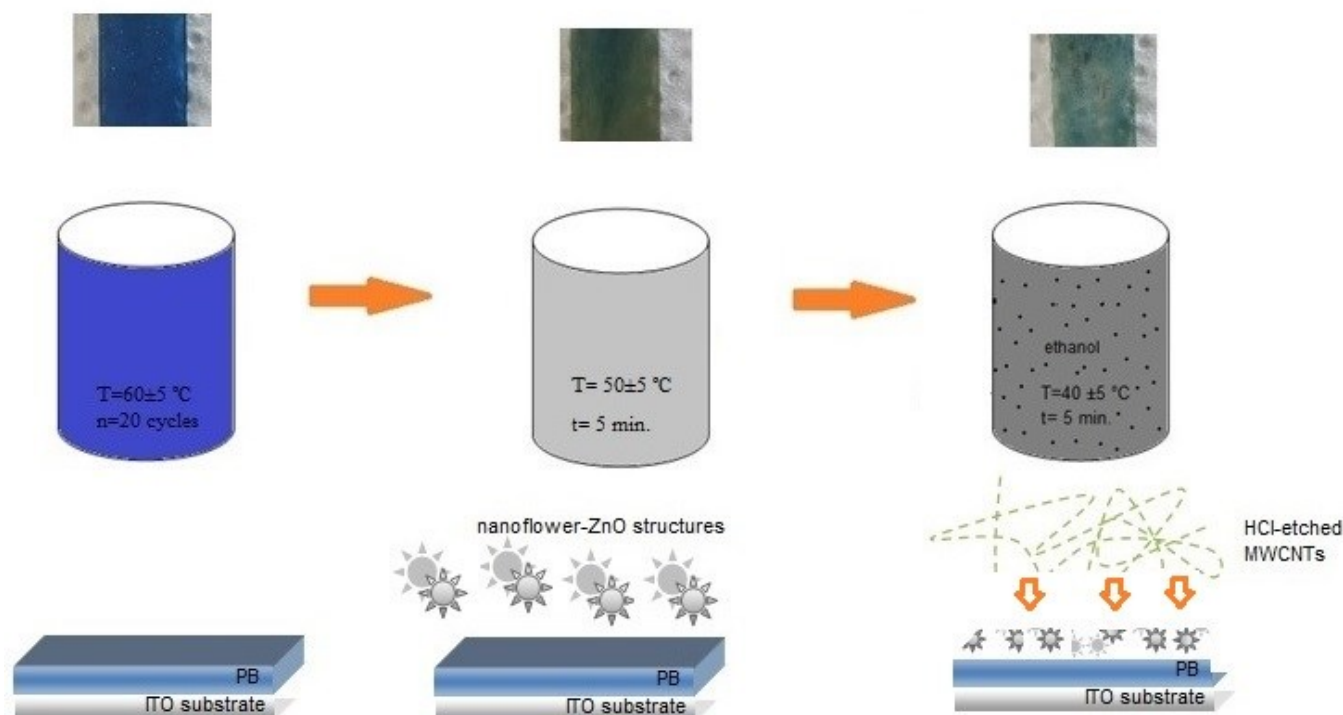


Figure 1. Schematic illustration of chemical bath deposited a) PB films b) PB-ZnO nanocomposite films and c) MWCNT decorated PB-ZnO (PB-ZnO/MWCNT) nanocomposite films, respectively.

hance surface functionalization, redox ability and electrochemical stability of host matrix [6]. On the other hand, properties of nanocomposites changes due to the chemical interactions, solubility of components and compatibility of mixing materials thereby growth technique.

Many physical (molecular beam epitaxy, magnetron sputtering, vacuum evaporation etc.) and chemical (spin coating, chemical vapor deposition, spray pyrolysis etc.) film growth techniques have been given in the literature depending on the material type and application field of this material [7]. Chemical bath deposition is an aqueous solution based technique which has attractive properties such as cheap and simple set-up system, short-term acquisition, non-vacuum process, applicable on the large surfaces and suitability for a lot of semiconductors. However, to get adhesive and smooth surface are still problems in that technique.

So many approaches have been used to prepare PB-MWCNT nanocomposites for investigation of their optical and electrochemical properties. Nossol et.al. (2012) showed that stability and redox properties of PB were improved by controlled amount of CNTs due to PB nanocubes have heterogeneous reactions with CNT walls PB/CNT films have relatively low optical contrast but CNT- incorporation was improved electrochromic performance and electrochemical stability while compared to bare-PB film (2012) [8]. Average size of PB nanoparticles were found to be 40 nm. which have been formed on CNT surfaces and they exhibited electrocatalytic activity towards H_2O_2 reduction as explained by Zhai et.al. (2009) [9]. A study received by Du et.al. (2010) reported that MWCNTs

had an effect on the enhanced electrode-specific capacitance and increased electron-ion transfer with by using one-step electrochemical co-deposition method (2010) [10].

According to our knowledge, there have been no report about PB-ZnO or MWCNT decorated PB-ZnO nanocomposite films. The aim of this work was to understand electrochemical and optical properties of PB-ZnO and MWCNT decorated PB-ZnO nanocomposite films (PB-ZnO/MWCNT) that deposited by chemical bath at low temperature.

2. SYNTHESIS AND CHARACTERIZATION OF NANOCOMPOSITES

2.1. Synthesis

Before the deposition process In-doped SnO_2 (ITO) substrates were cleaned by ethanol and n-hexane, then substrates were dried in air ambient conditions along one day. All chemicals obtained from Sigma-Aldrich without further purification. The PB films were prepared by using the experimental procedure of Velevska et.al.(2016) [11]. PB seed layers were dipped into Zn-based alkaline solution. ZnO film preparation method with modified chemical bath deposition was explained in our previous report (2017) [12]. PB films had a blue color whereas PB-ZnO nanocomposite films had a green color due to oxidation by ZnO as well as PB-ZnO/MWCNT nanocomposite films have had turquoise color when viewed with the naked eye, as seen in Fig. 1. MWCNTs contain 10% metal impurities purchased from Nanografi Company/METU. HCl acid-etching technique was applied to MWCNTs by mixing

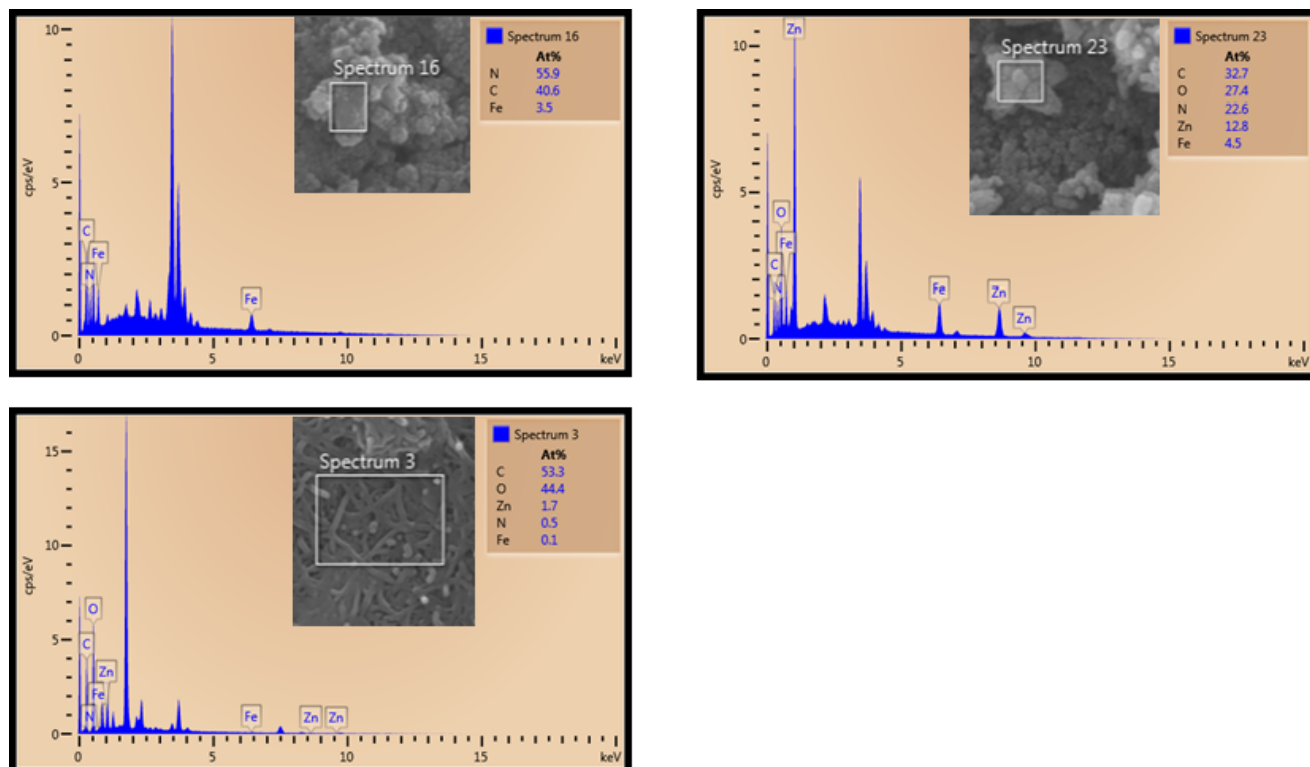


Figure 2. EDX analysis results of a) PB films b) PB-ZnO nanocomposite films and c) PB-ZnO/MWCNT nanocomposite films, respectively. (* and \$ marking corresponds to Si- and Ca- elemental peak related to ITO substrate, respectively).

them into ethanol bath to increase the solubility of MWCNTs. PB/ZnO nanocomposite films were immersed into that solution for about 5 minutes. Optimum working temperature was determined at 40 ± 5 °C for to synthesize MWCNT decorating PB-ZnO film synthesis. Finally, nanocomposite films were dried at 120 °C in the furnace under un-vacuum ambient.

2.2. Characterization

The surface morphology of the samples was observed by JEOL JSM-7100F-SEM (scanning electron microscope). Elemental analysis of the samples was determined by OXFORD Instruments X-Max EDX (energy-dispersive x-ray spectrometer) which had been attached to SEM. To understand the electroactivity of all nanocomposite films, cyclic voltammetry (CV) and electrochemical impedance spectroscopy (EIS) equipments were used. Electrochemical experiments were realized standart three-electrode configuration with reference electrolyte type and scan rate was chosen 0.1 M $(\text{Fe}(\text{CN})_6)^{3-/4-}/\text{KCl}$ and 50 mV/s, respectively. Impedance curves were performed using a Compactstat Interface (Ivium Technologies -Eindhoven, The Netherlands) and Autolab PGSTAT 128N Potentiostat/Galvonstat equipped with a FRA2 frequency response analyzer. A part of optical properties of the samples investigated by Analytic Jena Uv-Vis spectrometer which was recorded in the range of 300-900 nm. The Raman spectra was obtained by using Thermo DXR Raman spectrophotometer with measured in the range between 100- and 3000 cm^{-1} which excited with the 780 nm laser line. FTIR (Fourier Transform Infrared Spectrum) measure-

ments were recorded on VERTEX 70 model spectrophotometer with an attenuated total reflectance (ATR) accessory in the range of 400- and 4000 cm^{-1} (Bruker, Germany). All measurements were conducted at room temperature.

3. RESULTS AND DISCUSSION

3.1. Elemental Analysis Results

To confirm the successful nanocomposite film synthesis, elemental composition was determined by EDX and the obtained results showed in Fig.2. All films had adhesive property since impurity or ITO-based elemental ratio were not determined. As expected, PB films had highly higher nitrogen and carbon and relatively low iron elemental ratios as shown in Fig.2.(a). The highest zinc elemental ratio is was detected in PB-ZnO nanocomposite films with due to the entrance of Zn^{2+} ions in the PB-lattice as seen in Fig.2.(b). Moreover, the highest carbon elemental ratio was detected in PB-ZnO/MWCNT nanocomposite films because of coating of carbon atoms on the PB-ZnO surface as seen in Fig.2.(c). All the films had higher oxygen ratio due to the OH^- groups in alkaline solution during deposition process which was reported by Allouche et. al. (2010) [13]. Additionally, CNT surfaces gained much more oxygen-containing functional groups for in PB-ZnO/MWCNT nanocomposite films which was investigated by Yao et.al. (2012) [14].

3.2. Surface Morphology Images

The surface morphology and expected formation of nanocompo-

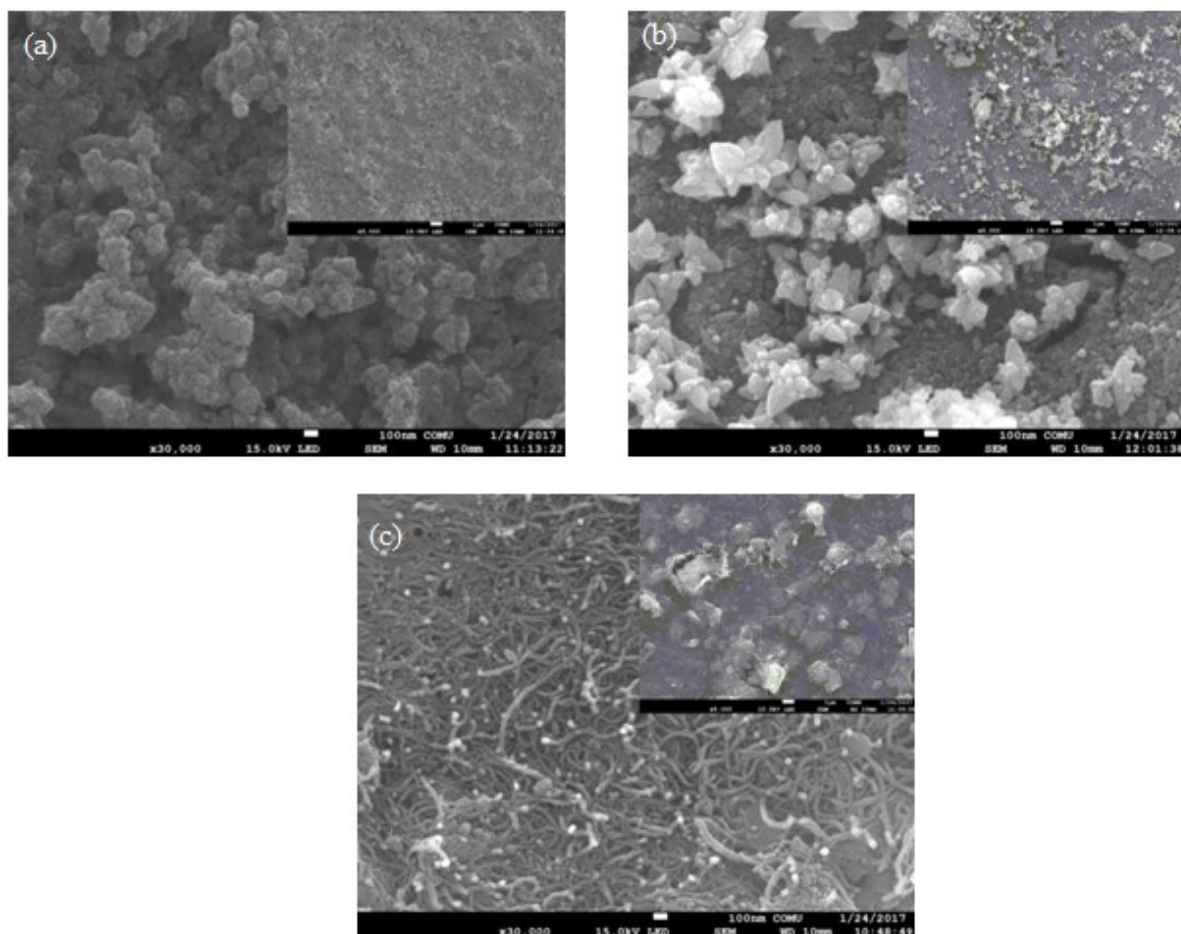


Figure 3. SEM images of a) PB films b) PB-ZnO nanocomposite films and c) PB-ZnO/MWCNT nanocomposite films, respectively.

sites were confirmed by scanning electron microscope (SEM) and average structure sizes were estimated. As seen in SEM images of nanocomposites, adhesive films were obtained. Fig.3 (a) showed that sphere-shaped and low percentage cubic-shaped PB nanoparticles which have been distributed onto ITO surface, randomly. Their dimensions were changed between in 30- and 100 nm. range. It is known that PB nanoparticles have been formed with a mixture of ferric (Fe^{3+}) and ferricyanide ($\text{Fe}(\text{CN})_6^{4-}$) ions. Cubic formations generally can emerge in ferricyanide ($\text{Fe}(\text{CN})_6^{4-}$) ion ambient [15]. A small number of nano-flower shaped ZnO particles connected to sphere-shaped PB particles as seen in Fig.3 (b). In PB-ZnO nanocomposite, sphere shaped PB particle sizes were smaller than in PB film. In addition, their dimensions have been decreased to (~15-20 nm.) but however agglomerative ZnO formation dimensions were bigger than PB particles due to the higher concentration of the precursor solution [16]. In Fig.3(c), spaghetti-like arranged MWCNTs which had diameters of 18-24 nm. range almost completely coating coated on PB-ZnO films. That enhanced surface lead an increase on electron transfer process [17].

3.3. Electrochemical Properties

3.3.1. Cyclic Voltammetry (CV) Measurements

Cyclic voltammetry (CV) is an useful tool to understand kinetic

redox reactions. and CV measurement results were given in Fig.4. ZnO or ZnO/MWCNT modification altered the oxidation and reduction processes of PB films. Salazar et.al. (2012) explained that PB was un-stable in alkaline solutions so electro-catalytic activity was loosed which indicated the transformation of $\text{Zn}(\text{OH})_2$ to pure ZnO (2012) [18].

Typical peaks about PB ($\text{Fe}^{\text{III}}\text{Fe}^{\text{II}}$ species) electrochemical transformation (reduction Fe^{3+} to Fe^{2+}) to PW (prussian white) ($\text{Fe}^{\text{II}}\text{Fe}^{\text{II}}$ species) and PB ($\text{Fe}^{\text{III}}\text{Fe}^{\text{II}}$ species) electrochemical transformation (oxidation Fe^{2+} to Fe^{3+}) to PG (Prussian green) ($\text{Fe}^{\text{III}}\text{Fe}^{\text{III}}$ species) peaks were observed in Fig.4 (black colored) [19].

In Fig.4., no PB-PW transformation was detected (irreversible situation) for PB-ZnO and PB-ZnO/MWCNT electrodes because of OH^- groups might be caused being different type defects, Zn^{2+} ions might be substituted with Fe^{2+} sites and ferricyanide ions might be bonded to oxygen containing functional groups with increasing HCl-etched MWCNT stress which indicate surface defects and voltammetric conditions severely affected the electrochemical behaviour [20]. The relative peak current increase was observed during nanocomposite forming which indicated a continuous deposition of the material on PB films in alkaline medium. On the other hand, the alteration of anodic peak current was specified by electron diffusion behaviour which was investigated by Thakur et.al.

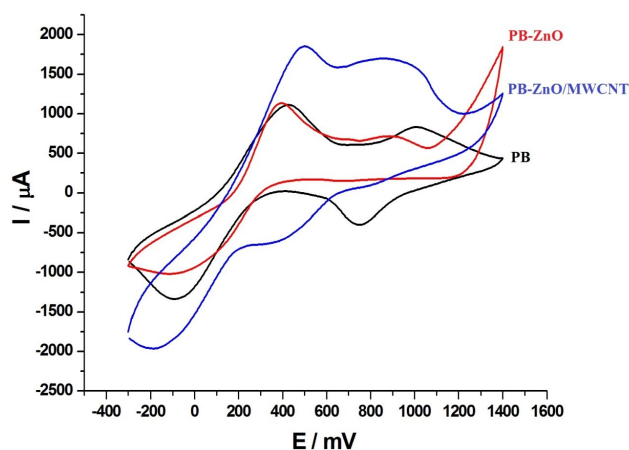


Figure 4. Cyclic voltammograms of PB films (), PB-ZnO nanocomposite films () and PB-ZnO/MWCNT () nanocomposite films. Cyclic voltammetry measurements were realized conducted with 0.1 M $(\text{Fe}(\text{CN})_6)^{3-/4-}/\text{KCl}$ as probe at a scan rate of 50 mV/s.

(2017) [21]. Anodic peak increasing was higher in PB-ZnO/MWCNT nanocomposite electrode compared to PB-ZnO electrode. This could be explained in two ways; the first one is increasing reaction kinetics depending on the enhanced active surface area which was confirmed by SEM images and the second one is removal of zinc atoms from the surface of PB-ZnO/MWCNT structures which was confirmed by EDX results. Table 1 listed the potential and current data about deposited nanocomposites. Because of the improvements of the redox reversibility, ratio of peak current (I_{pa}/I_{pc}) in PB-ZnO/MWCNT electrode decreased obviously compared to PB electrode.

3.3.2. Electrochemical Impedance Measurements

Electrochemical impedance spectroscopy has given an evidence of additional material effect on the PB electro-active surface. In Fig. 5., electrochemical impedance spectroscopy of electrodes were given with a circuit diagram in where R_s , R_{et} , W , C were corresponding to ohmic resistance, electron charge transfer resistance, Warburg impedance and double layer capacitance, respectively. The real variable and the negative value of the imaginary variable of impedance were depicted by Z' and Z'' . Ohmic resistance (while $Z'' = 60 \Omega$ $Z' = 0$) remained almost constant due to the high conductive nature of materials [22]. Nyquist plots consists of two parts, one is semicircle in high frequency region which is about the charge transport and another one is Warburg line in low-frequency region which is about the diffusion process [23]. As can be seen in Fig.5., PB samples were exhibited small semicircle

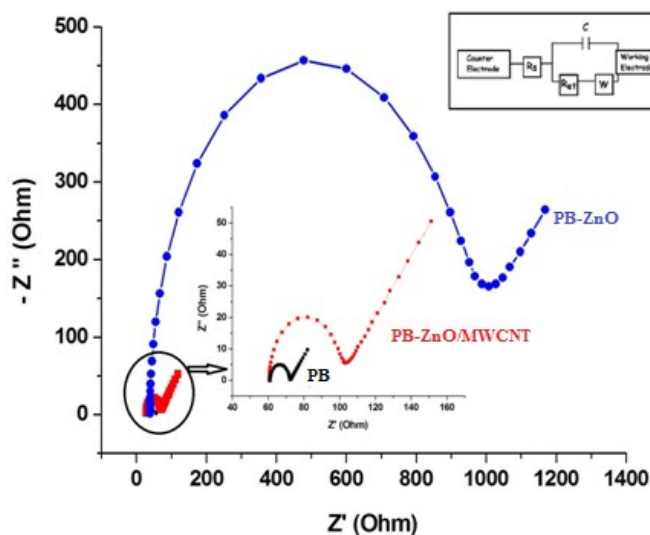


Figure 5. Nyquist plots of PB (black), PB-ZnO (blue) and PB-ZnO/MWCNT (red) nanocomposite films in 10.0 mM $(\text{Fe}(\text{CN})_6)^{3-/4-}$ solution contains 0.10 M KCl in Faradaic mode at the formal potential of +0.18 V with the frequencies swept from 10000 to 0.1 Hz and signal amplitude 5 mV at room temperature.

at high frequency region and this semicircle was enhanced for PB-ZnO/MWCNT and after semicircle that having the maximum radius was observed for PB-ZnO, implying its maximum resistance. The electron charge transfer resistance (R_{et}) was dramatically increased from PB to PB-ZnO/MWCNT and then from PB-ZnO/MWCNT to PB-ZnO ($R_{et}(\text{PB}) < R_{et}(\text{PB-ZnO/MWCNT}) < R_{et}(\text{PB-ZnO})$). Zn^{2+} ions were adversely affected the charge transport process and these results were confirmed by CV results. As explained by Mendez et.al. YIL that charge transport phenomena was related to redox reactions for electronic charge transport [24]. Warburg line extrapolation in the low frequency's limit gave the double layer capacitance at the ITO/coated sample interface and this value was similar for all samples (45°) which indicated adding material in the host matrix was not important in the diffusion process.

3.4. Optical Properties

3.4.1. Uv-Vis Spectroscopy

In Fig. 6., Uv-Vis spectra of nanocomposites were showed shown in the range of 300-900 nm. PB- and PB-ZnO/MWCNT nanocomposite films showed similar optical behaviour in the visible region and their transparency were so close which was higher than 50%. Whereas, PB-ZnO films had low transparency due to increasing agglomerative formations and nanocomposite film thick-

Table 1. Cyclic voltammogram datas for PB, PB-ZnO and PB-ZnO/MWCNT nanocomposite films

Nanocomposite type	Anodic peak potential (V) (E_{pc})	Cathodic peak potential (V) (E_{pa})	Anodic peak current (10^{-4} A) (I_{pc})	Cathodic peak current (10^{-4} A) (I_{pa})	Peak potential separation (mV)
PB	0.435	-0.075	8.3056	-7.7053	50
PB-ZnO	1.000	0.700	6.2651	-2.1806	50
PB-ZnO/MWCNT	0.555	-0.150	3.9837	-4.2496	50

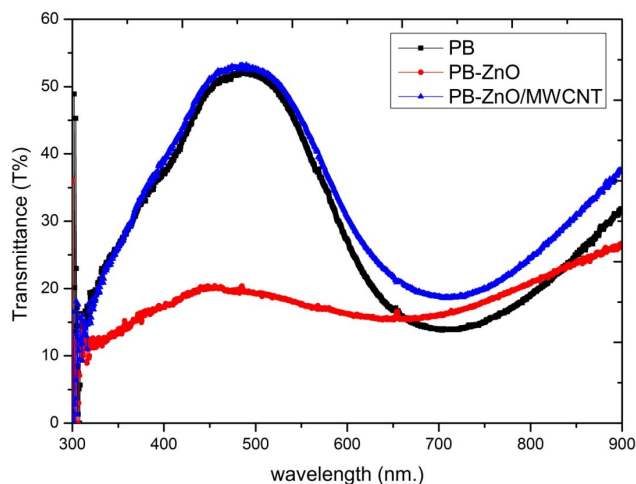


Figure 6. UV-Vis spectra of PB films (blue), PB-ZnO nanocomposite films (red) and PB-ZnO/MWCNT nanocomposite films (black).

ness, as can be seen in SEM images. PB- and PB-ZnO/MWCNT nanocomposite films had characteristic PB broad absorption peak approximately at 720 nm, which indicated the mixed valance charge transfer of Fe^{2+} -CN- Fe^{3+} with a good agreement in the literature with removal of zinc atoms from the surface for PB-ZnO/MWCNT structures that obtained by EDX analysis results [25]. This band was shifted to short-wavelength (at 650 nm.) and band broadening was observed for PB-ZnO nanocomposite films. Two impurity originated fluctuations were observed approximately at 485 nm. (2.55 eV) and at 655 nm. (1.89 eV) especially in PB-ZnO films due to increasing surface defects which was reported by Dutta et.al. (2014) [26]. However, PB-ZnO/MWCNT nanocomposites did not have impurity with optical improving effect of MWCNT.

3.4.2. FTIR Spectroscopy

Fig.7. shows the FTIR transmission spectrum of three different nanocomposites in the range of 400 cm^{-1} to 4000 cm^{-1} . In PB-ZnO nanocomposites, broadening on the peak positions was detected due to the increasing stress in the PB lattice depending on atom positions and changing morphology with Zn^{2+} ion inclusion. All samples had characteristic two PB peaks which that one of them was positioned at 2068 cm^{-1} (stretching vibration mode of $\text{C}\equiv\text{N}$ group) and another one was positioned at 592 cm^{-1} (Fe^{2+} -CN- Fe^{3+} linkage) [27]. The sharp peak around 470 cm^{-1} was attributed to Zn-O stretching vibration mode and that peak was evidently observed in PB-ZnO and PB-ZnO/MWCNT nanocomposites [28]. Decreased intensity of this peak was observed with entering of MWCNTs due to the reduction of Zn^{2+} ions in the structure which was confirmed by EDX results. Alkaline medium effect can be determined in PB-ZnO nanocomposites which was positioned at 3350 cm^{-1} (stretching vibration mode of O-H) [29]. The peak at 1554 cm^{-1} was due to C=C stretching mode of the CNT and this is was an evidence of existing MWCNTs [30]. Therefore, the presence of PB, ZnO and MWCNT were identified by FTIR spectra depending on nanocomposite types.

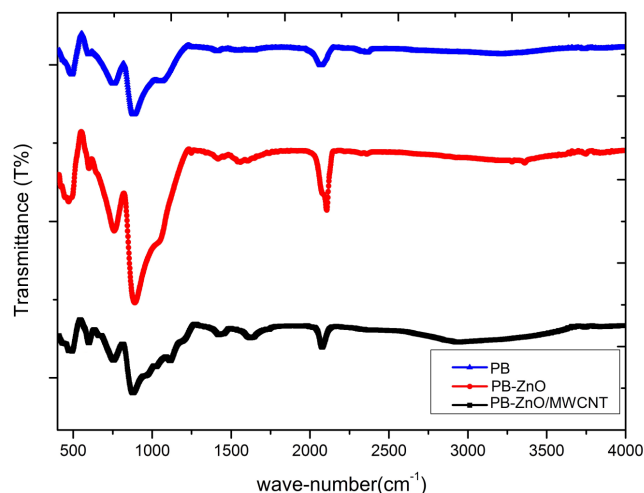


Figure 7. FTIR spectra of PB films (blue), PB-ZnO films (red) and MWCNT decorated PB-ZnO films (black).

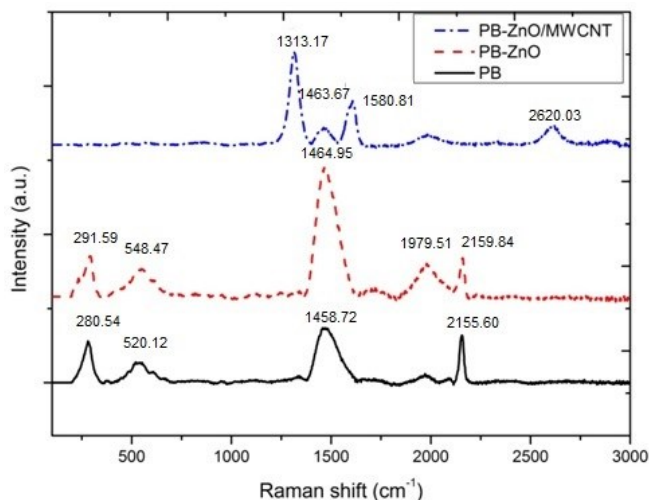


Figure 8. Raman spectra of PB films (-), PB-ZnO films (---) and MWCNT decorated PB-ZnO films (-·-·-). Alta kayakak

3.4.3. Raman Spectroscopy

Detailed analysis of Raman spectra of three different nanocomposites is showed in Fig.8. It gives an information about the interaction between nanocomposite parts and morphological disorder depending on the behaviour of optical phonons. Characteristic PB related peak was coordinated at 2155.60 cm^{-1} and appeared by the stretching vibration of $\text{C}\equiv\text{N}$ which was relatively confirmed by FTIR results [31]. This peak was shifted at 2159.84 cm^{-1} with introducing Zn^{2+} ions in the structure which may be explained by two ways. One was increasing tensile strain in the PB-ZnO film and another one was decreasing PB nanoparticle sizes with correlated to increasing grain boundaries which was confirmed by SEM images [32]. On the other hand, this peak disappeared by MWCNT coating on the PB-ZnO surface. It indicated that MWCNT coverage might cause a structural distortion. Similar explanation might be

done for ZnO-based peaks (at 548.47 cm^{-1} and 1979.51 cm^{-1}) in PB-ZnO nanocomposites. Peaks at 280.54 and 1458.72 cm^{-1} were proved the presence of PB nanoparticles especially originated from deformation of Fe-C-N vibrations [33]. Due to the random orientation, a relatively broad peak was observed at 548.47 cm^{-1} which was associated by $A_1(\text{LO})$ mode of ZnO and it was a prove for presence of ZnO structure [34]. A weak peak was centered obviously at 1979.51 cm^{-1} for PB-ZnO samples, its intensity and broadening were so low in other samples which was probably generated by defects at the grain boundaries [35]. Zn-interstitial defect-based ($\sim 552 \text{ cm}^{-1}$) and oxygen vacancy-based ($\sim 750 \text{ cm}^{-1}$) bands were not detected [36,37] which means high quality film formation in PB-ZnO and PB-ZnO/MWCNT nanocomposites. Typical MWCNT bands were detected at 1580.81 cm^{-1} (G-band) and 1313.17 cm^{-1} (D-band). G band and D-band were corresponding to sp^2 -hybridized carbon and amorphous/disordered carbon, respectively [38]. D-band shifting to short-wave number was observed due to the increasing of oxygen containing functional groups and reduction of MWCNT surface metals with HCl-etching. Additionally, weak G' (2D) band was observed at 2620.03 cm^{-1} which was originated from characteristic C-H vibrations with sp^2 - and sp^3 -hybridization [39].

4. CONCLUSIONS

The PB, PB-ZnO and PB-ZnO/MWCNT nanocomposite films have been successfully and adherently deposited by simple chemical bath onto ITO substrates. Optical and electrochemical properties of the nanocomposites were investigated detailed. SEM images showed that nanoflower shaped nanoparticles hold on to some PB nanoparticles and also MWCNTs entirely coated onto PB-ZnO surface. While PB-ZnO nanocomposite films were more adherent than PB films, whereas electrochemical stability and optical transparency of PB-ZnO films were so low due to hydroxyl groups and agglomerative formations depending on these groups. In spite of this, MWCNT decorating had a facilitate effect on optical and electrochemical properties of on PB- ZnO nanocomposite films.

REFERENCES

- [1] Cai, G., Wang, J., Lee, P., *Acc. Chem. Res.*, (2016). Doi: 10.1021/acs.accounts.6b00183.
- [2] Yang, P., Sun, P., Mai, W., *Materials Today*, (2016). Doi: 10.1016/j.mattod.2015.11.007.
- [3] Lee, E., DiBartolomeo, D.L., Klems, J.H., Yazdanian, M., Selkowitz, S.E., *ASHRAE Transactions*, 1 (2006).
- [4] Hu, M., Belik, A.A., Imura, M., Mibu, K., Tsujimoto, Y., Yamauchi, Y., *Chem. Mat.*, (2012). Doi: 10.1021/cm300615s.
- [5] Adaka, S., Hart, M., Daemenc, L., Fohntunga, E., Nakotte, H., *Journal of Electron Spectroscopy and Related Phenomena*, (2017). Doi: 10.1016/j.elspec.2016.11.011.
- [6] Abu-Salah, K.M., Alrokyan, S.A., Khan, M.N., Ansari, A.A., *Sensors*, (2010). Doi: 10.3390/s100100963.
- [7] Kemell, M., Ritala, M., Leskelä, M., *Critical Reviews in Solid State and Materials Sciences*, (2005). Doi: 10.1080/104084305-90918341.
- [8] Nossol, E., Zarbin, A.J.G., *J. Mater. Chem.* (2012). Doi: 10.1039/c1jm14225a.
- [9] Zhai, J., Zhai, Y., Wen, D., Dong, S., *Assembly and Electrochemical Behavior. Electroanalysis* (2009). Doi: 10.1002/elan.200904680.
- [10] Du, D., Wang, M., Qina, Y., Lin, Y., *J. Mater. Chem.*, (2010). Doi: 10.1039/b919500a.
- [11] Velevska, J., Pecovska-Gjorgjevich, M., Stojanov, N., Najdoski, M., *Basic and Applied Research*, 25, 380 (2016).
- [12] Özütok, F., Demiri, S., *Digest Journal of Nanomaterials and Biostructures*, 12, 309 (2017).
- [13] Allouche, N.K., Nasr, T.B., Kamouna, N.T., Guasch, C., *Materials Chemistry and Physics*, 123, 620 (2010).
- [14] Yao, Y., Bai, X., Shiu, K., *Nanomaterials*, (2012). Doi: 10.3390/nano2040428.
- [15] Prabakar, S.J.R., Jeong, J., Pyo, M., *RSC Advances*, (2015). Doi: 10.1039/c5ra04769b.
- [16] Jomma, E.Y., Ding, S., *Sensors*, (2016). Doi: 10.3390/s16020243.
- [17] Salavagione, H.J., Díez-Pascual, A.M., Lazaro, E., Verab, S., Gómez-Fatou, M.A., *J. Mater. Chem. A*, (2014). Doi: 10.1039/c4ta02159b.
- [18] Salazar, P., Martín, M., O'Neill, R.D., Roche, R., González-Mora, J.L., *Int. J. Electrochem. Sci.*, 7, 5910 (2012).
- [19] Haghghi, B., Hamidi, H., Gorton, L., *Sensors and Actuators B*, (2010). doi:10.1016/j.snb.2010.03.020.
- [20] Das, R., Md. Ali, Hamid, S.B.A., Annuar, M. S. M., Ramakrishna, S.: *Common Wet Chemical Agents for Purifying Multiwalled Carbon Nanotubes. Journal of Nanomaterials* (2014). Doi: 10.1155/2014/945172.
- [21] Thakura, B., Xiaoru Guo, Jingbo Chang, Michael Kron, Junhong Chen, *Sensing and Bio-Sensing Research*, (2017). Doi: 10.1016/j.sbsr.2017.05.002.
- [22] Stević, Z., Vujasinović, M.R., Radunović, M., *Sensors* (2009). doi:10.3390/s90907365.
- [23] Klapiszewski, L., Szalaty, T.J., Kurc, B., Staniszc, M., Skrzypczak, A., Jesionowski, T., *Int. J. Mol. Sci.*, (2017). doi:10.3390/ijms18071509.
- [24] Mendez, P.F., Lopez, J.R., Lopez-Garc, U., Manríquez, J., Frontana, C., Rodríguez, F.J., Godínez, L.A., *Journal of The Electrochemical Society*, (2017). Doi: 193.255.97.46.
- [25] Farah, A. M., Billing, C., Dikio, C. W., Dibofori-Orji, A.N., Oyediji, O.O., Wankasi, D., Mtunzi, F.M., Dikio, D., *Int. J. Electrochem. Sci.*, 8, 12132 (2013).
- [26] Dutta, S., Chattopadhyay, S., Sarkar, A., Chakrabarti, M. Sanyal, D., Jana, D., *Progress in Materials Science* (2014). doi:10.1016/j.pmatsci.2008.07.002.
- [27] Reguera, E., Fernández-Bertrán, J., Nuñez, L., *Z. Naturforsch.* 50b, 1067 (1995).
- [28] Khan, Z.R., Khan, M.S., Zulfequar, M., Khan, M.S., *Materials Sciences and Applications* (2011). doi:10.4236/msa.2011.25044.
- [29] Fan, M., Dai, D., Huang, B., *Materials Analysis*, 260 (2012). ISBN 978-953-51-0594-7.
- [30] Noguchi, T., Kamimura, Y., Inoue, Y., Itoh, S., *Plant Cell Physiol.* 40, 305 (1999).

- [31] Kettle, S.F.A., Diana, E., Marchese, E.M.C., Boccaleric, E., Stanghellini, P.L., *J. Raman Spectrosc.*, (2011). Doi: 10.1002/jrs.2944.
- [32] Barsan, M.M., Butler, I.S., Fitzpatrick, J., Gilson, D.F.R., *J. Raman Spectrosc.*, (2011). Doi: 10.1002/jrs.2931.
- [33] Lisowska Oleksiak, A., Nowak, A.P., Jasulaitiene, V., *Electrochemistry Communications* 8, 107 (2006).
- [34] Reyes, J.D., Juárez, J.M., Hernández de la Luz, D., *Revista Colombiana de Materiales*, 5, 103 (2014).
- [35] Liu, X., Balla, I., Bergeron, H., Hersam, M.C., *J. Phys. Chem. C*, (2016). DOI: 10.1021/acs.jpcc.6b02073.
- [36] Ghose, S., Rakshit, T., Ranganathanc, R., Jana, D., *RSC Adv.* (2015). DOI: 10.1039/c5ra13846a.
- [37] Apopei, A.I., Buzgar, N., Buzatu, A., *Seria Geologie*, 57, 35 (2011).
- [38] Costa, S., Borowiak-palen, E., Kruszyńska, M., Bachmatuk, A., Kaleńczuk, R.J., *Materials Science-Poland*, 26, 433 (2006).
- [39] Zhang, N., Wang, G., Gu, A., Feng, Y., Fang, B., *Microchim. Acta*, (2010). Doi: 10.1007/s00604-009-0274-8.